GEOMETRIC LOW-RANK TENSOR APPROXIMATION FOR REMOTELY SENSED HYPERSPECTRAL AND MULTISPECTRAL IMAGERY FUSION

Na Liu, Wei Li and Ran Tao

School of Information and Electronics, Beijing Institute of Technology

ABSTRACT

Improving the spatial resolution of a hyperspectral image (HSI) is of great significance in the remotely sensed field. By fusing a high-spatial-resolution multispectral image (MSI) with an HSI collected from the same scene, hyperspectral and multispectral (HS–MS) fusion has been an emerging technique to address the issue. Extracting complex spatial information from MSIs while maintaining abundant spectral information of HSIs is essential to generate the fused high-spatial-resolution HSI (HS^2I). A common way is to learn low-rank/sparse representations from HSI and MSI, then reconstruct the fused HS^2I based on tensor/matrix decomposition or unmixing paradigms, which ignore the intrinsic geometry proximity inherited by the low-rank property of the fused HS^2I. This study proposes to estimate the high-resolution HS^2I via low-rank tensor approximation with geometry proximity as side information learned from MSI and HSI by defined graph signals, which we name GLRTA. Row graph $\mathcal{G}_r$ and column graph $\mathcal{G}_c$ are defined on the horizontal slice and lateral slice of MSI tensor $\mathcal{M}$ respectively, while spectral band graph $\mathcal{G}_b$ is defined on a frontal slice of HSI tensor $\mathcal{H}$. Experimental results demonstrate that the proposed GLRTA can effectively improve the reconstruction results compared to other competitive works.

Index Terms— Graph signal processing, hyperspectral imagery, low-rank tensor approximation, remote sensing, super-resolution

1. INTRODUCTION

Due to an inevitable tradeoff between spatial and spectral resolution in optical imaging systems, remotely sensed hyperspectral imagery (HSI) suffers poor spatial resolution, while multispectral imagery (MSI) typically has high spatial resolution. Consequently, using MSI to enhance the spatial resolution of HSI is of great interest in remote sensing field [1].

The key to a successful HS-MS fusion can be summarized as two-folds: an effective spatial and spectral information learning strategy and an elaborated fusion framework that can combine the learned spatial and spectral information to generate the fused HS^2I [2]. As a high-order multi-way representation, tensor is one of such techniques that has been increasingly brought to bear on the HS-MS fusion task, which can preserve the spatial-spectral dependence within the image cube [1, 3]. A popular strategy is to deploy different tensor decomposition [1, 2, 4–7] with tedious regularization terms, such as the well-known patch-based non-local similarity learning[8] and dictionary-learning schemes [1]. While such tensor-decomposition approaches to HS-MS fusion can yield effective results, they tend to be fraught with several difficulties, including the well-known nonuniqueness of the decomposition [9](leading to an inequivalent to Parseval's theorem [3]), as well as the high computational complexity entailed in learning the decomposed components.

To circumvent the difficulties outlined above surrounding tensor decomposition, a geometric tensor-trace-norm formulation is recast to drive HS-MS fusion, producing an HS^2I cube that couples the spatial structure of the constituent MSI with the spectral relationship from the HSI. The resulting geometric low-rank tensor-approximation (GLRTA) algorithm imposes a low-rank tensor trace norm [10] directly on the target HS^2I cube. In addition, spatially geometric side information and spectral proximity similarity are transferred from HSI and MSI to maintain the integrity of the fused HS^2I by defining graph signal on each mode, which is efficient to learn the hidden geometry information inherited by low-rank constraints. Besides, graph based similarity learning avoids the computationally complex patch clustering and dictionary learning common to existing techniques by spectral analysis methods. The proposed GLRTA based HS-MS fusion method also shares the advantage that it doesn't need observation indicators to solve the approximation optimization based fusion problem, the spatial/spectral response functions are readily used for the information preservation and diffusion from HSI and MSI to the constructed HS^2I.

2. PROPOSED HS-MS FUSION ALGORITHM

Geometric analysis of matrix completion (GMC) has been well studied in spectral graph signal processing field [11, 12], which has been widely used in disease prediction [13] and recommendation system [14], etc. However, for high-order

This work is supported by the Beijing Natural Science Foundation (Grant no. JQ20021), the China Postdoctoral Science Foundation (Grant no. 2021M700440), National Natural Science Foundation of China(Grant no. 61922013). (Corresponding author: Wei Li, Email: liwei089@ieee.org)

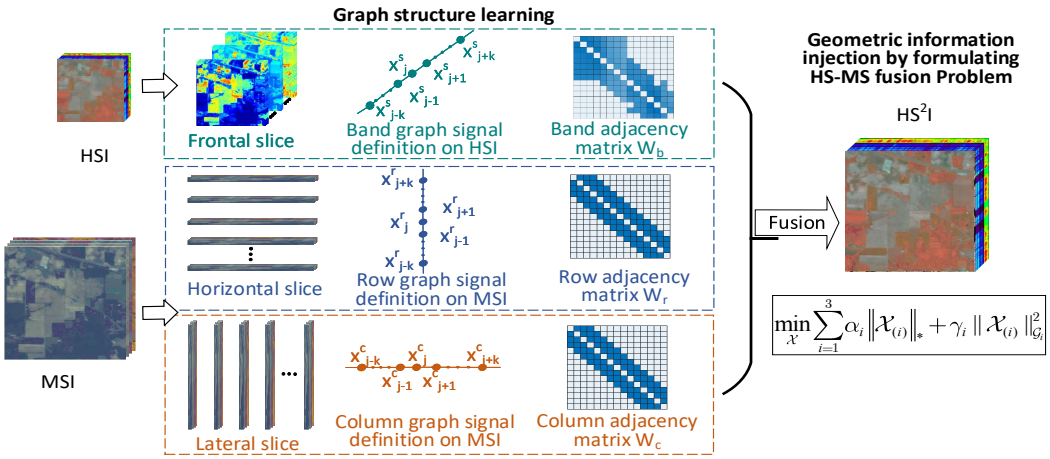

Fig. 1. Graph signal definition on MSI and HSI for HS-MS fusion.

tensor completion problem, especially for HS-MS fusion (to estimate the fused HS^{2}I), to our best knowledge, it's the first time that geometric tensor-trace-norm approximation based on GMC is developed. Following we will describe the formulation of our proposed algorithm after a short introduction of the related work.

2.1. Mathematical Preliminaries

A real-valued order-n tensor is denoted as $\mathcal{X} \in \mathbb{R}^{I_1 \times \cdots \times I_k \times \cdots \times I_n}$, with each element being $x_{i_1,\ldots,i_k,\ldots,i_n}$, where I_k is the dimension of mode k, $1 \leq k \leq n$. The "**unfold**" operation along mode k is defined as $\mathbf{unfold}_k(\mathcal{X}) = \mathcal{X}_{(k)} \in \mathbb{R}^{I_k \times (I_1 \cdots I_{k-1} I_{k+1} \cdots I_n)}$. Correspondingly, the "**fold**" operation reverses the unfolding, $\mathbf{fold}_k(\mathcal{X}_{(k)}) = \mathcal{X}$. We also define the Frobenius norm of a tensor as $\|\mathcal{X}\|_F = (\sum_{i_1,\ldots,i_n} |x_{i_1,\ldots,i_n}|^2)^{\frac{1}{2}}$ such that $\|\mathcal{X}\|_F = \left\|\mathcal{X}_{(k)}\right\|_F$, $1 \leq k \leq n$. The multiplication of a tensor $\mathcal{X}$ with a matrix $\mathbf{A} \in \mathbb{R}^{J_k \times I_k}$ on mode k is defined by $\mathcal{Y} = \mathcal{X} \times_k \mathbf{A}$, where $\mathcal{Y} \in \mathbb{R}^{I_1 \times \cdots \times I_{k-1} \times J_k \times I_{k+1} \times \cdots \times I_n}$ and $y_{i_1,\ldots i_{k-1},j_k,i_{k+1},\ldots,i_n} = \sum_{i_k=1}^{I_k} x_{i_1,\ldots,i_k,\ldots,i_n} a_{j_k,i_k}$. Alternatively, after an **unfold** operation along mode k, the multiplication is defined as $\mathcal{Y}_{(k)} = \mathbf{A}\mathcal{X}_{(k)}$. Trace norm is defined as $\|\mathcal{X}\|_* = \sum_{k=1}^{n} \alpha_k \left\|\mathcal{X}_{(k)}\right\|_*$, where $\|\cdot\|_*$ is the matrix spectral norm and $\alpha_k \geq 0$ are weights such that $\sum_{k=1}^{n} \alpha_k = 1$.

2.2. Graph Signal Processing

Signal processing on graph (GSP) is an effective approach to describe and process high-dimensional data [15]. Let an undirected and weighted graph be defined as $\mathcal{G}=(\mathcal{V}, \mathcal{E}, \mathbf{W})$, where $\mathcal{V}$ and $\mathcal{E}$ denote the sets of vertices and edges of the graph, respectively; $\mathbf{W}$ denotes the weight matrix of edge. The degree of $v_i \in \mathcal{V}$ is calculated as the sum of element values in the i-th column of $\mathbf{W}$, i.e., $d_i = \sum_{j=1}^{N} w_{ij}$. The degree matrix is a diagonal one $\mathbf{D} = diag(d_1, d_2, ..., d_i, ..., d_N)$. The Laplacian matrix is defined as $\mathbf{L} = \mathbf{D} - \mathbf{W}$. Without loss of generality, given a graph $\mathcal{G}$, the graph signal is defined on the vertices of the graph $f : \mathcal{V} \to \mathbb{R}$.

2.3. Matrix Completion on Graph

An intuition to the low-rank constraint on a given matrix $\mathbf{M}$ is that there is some linear dependence between its rows/columns [16]. We define the simplest column graph $\mathcal{G}_c=(\mathcal{V}_c, \mathcal{E}_c, \mathbf{W}_c)$ of $\mathbf{M}$ to represent the proximity structure between columns with each column $\mathbf{x}_n$ being defined on v_n^c. The row graph $\mathcal{G}_r=(\mathcal{V}_r, \mathcal{E}_r, \mathbf{W}_r)$ is defined in a similar manner to represent the similarities of rows. The objective of matrix completion on graph (MCG) is to constrain the space of solutions in low-rank matrix completion problem to be smooth with respect to the geometric structure of the rows and columns of data defined on graph [12]. That it, MCG imposes the smoothness by setting $\mathbf{m}_j^c \approx \mathbf{m}_{j'}^c$, if $(j, j') \in \mathcal{E}_c$, and results in following formulation

$$\sum_{j,j'} w_{jj'}^c \left\|\mathbf{m}_j^c - \mathbf{m}_{j'}^c\right\|_2^2 = \mathbf{tr}\left(\mathbf{M}\mathbf{L}_c\mathbf{M}^\top\right) = \|\mathbf{M}\|_{\mathcal{G}_c}^2 \quad (1)$$

where $\mathbf{L}_c$ is the Laplacian of the column graph $\mathcal{G}_c$ and $\|\cdot\|_{\mathcal{G}_c}^2$ is the graph Dirichlet semi-norm for columns.

2.4. Proposed GLRTA based HS-MS Fusion

As shown in Fig. 1, to extract spectral and spatial information from the HSI $\mathcal{H} \in \mathbb{R}^{m \times n \times D}$ and MSI $\mathcal{M} \in \mathbb{R}^{M \times N \times d}$, graph signals are defined respectively. A spectral band graph $\mathcal{G}_b$ is defined on the HSI, where each frontal slice $\mathcal{H}(:,:,j)$ is denoted as a signal $\mathbf{h}_j^s$ on the vertex v_j^s of $\mathcal{G}_b$. Spatial row

graph $\mathcal{G}_r$ and column graph $\mathcal{G}_c$ are defined on the MSI, corresponding horizontal $\mathcal{M}(j,:,:)$ and lateral $\mathcal{M}(:,j,:)$ slices are defined on the vertices v_j^r and v_j^c of $\mathcal{G}_r$ and $\mathcal{G}_c$, respectively.

Then, based on the defined graphs, the weight matrices $\mathbf{W}_b$ is constructed to learn the spectral similarity of HSI; $\mathbf{W}_r$ and $\mathbf{W}_c$ are also learned to represent the spatially adjacent constraints. To guarantee that the abundant spectral information of HSI and spatial details information of MSI are injected to the final fused HS^{2}I $\mathcal{X}$, the learned proximity matrices are used to constrain the formulation of $\mathcal{X}$. That is, $\mathcal{X}$ is estimated by

$$\begin{aligned}&\min_{\mathcal{X}} \sum_{k=1}^{3} \gamma_k \sum_{j,j'} w_{jj'}^k ||\mathbf{x}_j^k - \mathbf{x}_{j'}^k||_2^2 \\ &= \min_{\mathcal{X}} \sum_{k=1}^{3} \gamma_k \mathrm{tr}({\mathcal{X}_{(k)}}^T \mathbf{L}_{(k)} \mathcal{X}_{(k)}) \\ &= \min_{\mathcal{X}} \sum_{k=1}^{3} \gamma_k ||\mathcal{X}_{(k)}||_{\mathcal{G}_k}^2\end{aligned} \tag{2}$$

where $\mathbf{L}_{(k)}$ (with k denotes the three modes) is the Laplacian of the each graph; parameters γ_k controls the intensity of graph preservation constraints on each mode of the expected fusion result $\mathcal{X}$.

Additionally, as is common for HS-MS fusion, we also formulate the fusion problem as the estimation of a low-rank tensor under the consideration of the sensors' observation model. Specifically, the fusion process is recast as

$$\begin{aligned}&\min_{\mathcal{X}} \sum_{k=1}^{3} \gamma_k ||\mathcal{X}_{(k)}||_{\mathcal{G}_k}^2 + \alpha_k ||\mathcal{X}_{(k)}||_* \\ &s.t., \ \ \mathcal{X}_{(3)}\mathbf{D} = \mathcal{H}_{(3)} \ \text{ and } \ \mathbf{S}\mathcal{X}_{(3)} = \mathcal{M}_{(3)},\end{aligned} \tag{3}$$

where α_k controls the intensity of low-rank constraints on each mode, $\mathbf{S} \in \mathbb{R}^{d \times D}$ denotes a matrix spanned by a spectral response function (SRF) that constitutes a spectral downsampling process, while $\mathbf{D} \in \mathbb{R}^{MN \times mn}$ is a spatial degradation matrix encapsulating the hyperspectral sensor's spatial point-spread function (PSF).

2.5. Relation to Prior Work

The formulation (3) of the proposed GLRTA algorithm for HS-MS fusion takes advantage of geometric analysis of matrix completion and tensor-trace-norm approximation. Specifically, we extend MCG to tensor completion on graph (TCG). The literature [17] and [18] consider graph-regularized fusion methods, they still focus on the learning of the tensor decomposition with the graph regularization on the decomposed sub-spaces. While the proposed GLRTA is related to them, it defines the graph signals on MSI and HSI respectively, then transfers the learned geometry relationship to the final fused HS^{2}I to facilitate an effective and efficient fusion model, which has not considered in these earlier studies.

2.6. Optimization

Eq. 3 is convex optimization but it can not be solved directly via differential calculus as it contains non-differential terms and the elements in the tensor are interdependent. Consequently, we follow alternating direction method of multipliers (ADMM) paradigm to solve it. For $k \in \{1,2,3\}$, we introduce auxiliary variables $\mathbf{M}_k$ for $\mathcal{X}_{(k)}$. Additionally, we have Lagrange multipliers $\mathbf{Y}_1'$, $\mathbf{Y}_2'$, and $\mathbf{Y}_k$, where again $k \in \{1,2,3\}$, as well as penalty parameters μ, η, and β. This renders (3) separable such that it can be solved via ADMM. Specifically, we form the augmented Lagrangian

$$\begin{aligned}&\mathrm{L}_{\mu,\beta,\gamma}(\mathcal{X}, \mathbf{M}_1, \mathbf{M}_2, \mathbf{M}_3, \mathbf{Y}_1, \mathbf{Y}_2, \mathbf{Y}_3, \mathbf{Y}_1', \mathbf{Y}_2') = \\ &\sum_{k=1}^{3} \gamma_k ||\mathcal{X}_{(k)}||_{\mathcal{G}_k}^2 + \sum_{k=1}^{3} \alpha_k \|\mathbf{M}_k\|_* + \sum_{k=1}^{3} \left\langle \mathbf{Y}_k, \mathcal{X}_{(k)} - \mathbf{M}_k \right\rangle \\ &+ \left\langle \mathbf{Y}_1', \mathbf{M}_3\mathbf{D} - \mathcal{L}_{(3)} \right\rangle + \left\langle \mathbf{Y}_2', \mathbf{S}\mathbf{M}_3 - \mathcal{H}_{(3)} \right\rangle + \frac{\mu}{2} \sum_{k=1}^{3} \left\| \mathcal{X}_{(k)} - \mathbf{M}_k \right\|_{\mathrm{F}}^2 \\ &+ \frac{\beta}{2} \left\| \mathbf{M}_3\mathbf{D} - \mathcal{L}_{(3)} \right\|_{\mathrm{F}}^2 + \frac{\eta}{2} \left\| \mathbf{S}\mathbf{M}_3 - \mathcal{H}_{(3)} \right\|_{\mathrm{F}}^2.\end{aligned} \tag{4}$$

Optimization problem (3) is then solved iteratively via (4) with the following subproblems:

1) Update $\mathbf{M}_k$ for $k = 1$ and 2 via

$$\mathbf{M}_{k,t+1} = \arg\min_{\mathbf{M}_k} \alpha_k \|\mathbf{M}_k\|_* + \frac{\mu}{2} \left\| \mathcal{X}_{(k),t} - \mathbf{M}_k + \frac{\mathbf{Y}_{k,t}}{\mu} \right\|_{\mathrm{F}}^2. \tag{5}$$

Problems of the form of (5) have a closed-form solution via the singular-value thresholding operator [19].

2) Update $\mathbf{M}_3$:

$$\begin{aligned}&\mathbf{M}_{3,t+1} = \arg\min_{\mathbf{M}_3} \alpha_3 \|\mathbf{M}_3\|_* + \frac{\mu}{2} \left\| \mathcal{X}_{(3),t} - \mathbf{M}_3 + \frac{\mathbf{Y}_{3,t}}{\mu} \right\|_{\mathrm{F}}^2 \\ &+ \frac{\beta}{2} \left\| \mathbf{M}_3\mathbf{D} + \mathcal{L}_{(3)} + \frac{\mathbf{Y}_{1,t}'}{\beta} \right\|_{\mathrm{F}}^2 + \frac{\gamma}{2} \left\| \mathbf{S}\mathbf{M}_3 + \mathcal{H}_{(3)} + \frac{\mathbf{Y}_{2,t}'}{\gamma} \right\|_{\mathrm{F}}^2.\end{aligned} \tag{6}$$

(6) usually does not have a closed-form solution because $\mathbf{D}$ and $\mathbf{S}$ are not identities. We propose to linearize the quadratic terms coupled with an adaptive rule for updating the penalty parameter (LADMAP) to solve the problem.

3) Update $\mathcal{X}_{(k)}$ for $k \in \{1,2,3\}$:

$$\begin{aligned}&\mathcal{X}_{(k),t+1} = \arg\min_{\mathcal{X}_{(k)}} \sum_{k=1}^{3} \gamma_k ||\mathcal{X}_{(k)}||_{\mathcal{G}_k}^2 + \\ &\left\langle \mathbf{Y}_{k,t}, \mathcal{X}_{(k)} - \mathbf{M}_{k,t+1} \right\rangle + \frac{\mu}{2} \left\| \mathcal{X}_{(k)} - \mathbf{M}_{k,t+1} \right\|_{\mathrm{F}}^2.\end{aligned} \tag{7}$$

(7) is given by solving a linear system of equations with conjugate gradient (CG) algorithm. Then, $\mathcal{X}$ is computed via the average on the three modes.

4) Update $\mathbf{Y}_k$ for $k \in \{1,2,3\}$ as well as $\mathbf{Y}_1'$, and $\mathbf{Y}_2'$:

$$\mathbf{Y}_{k,t+1} = \mathbf{Y}_{k,t} + \mu \left(\mathcal{X}_{(k),t+1} - \mathbf{M}_{k,t+1} \right), \tag{8}$$

$$\mathbf{Y}_{1,t+1}' = \mathbf{Y}_{1,t}' + \beta \left(\mathbf{M}_{3,t+1}\mathbf{D} - \mathcal{L}_{(3)} \right), \tag{9}$$

$$\mathbf{Y}_{2,t+1}' = \mathbf{Y}_{2,t}' + \gamma \left(\mathbf{S}\mathbf{M}_{3,t+1} - \mathcal{H}_{(3)} \right). \tag{10}$$

3. EXPERIMENTAL STUDY

One of the most important advantages of the proposed GLRTA is simple and easy to interpret. We also explain that the proposed model is efficient and generally extended by developing other low-rank tensor approximation models and graph based geometry preserving schemes.

In the proposed GLRTA, three groups of parameters must be considered: trace-norm parameters α_k; graph preserving parameters γ_k; penalty parameters μ, β and γ. We simply fix penalty parameters μ, β and γ as 0.001, 0.5 and 0.5, respectively. The α_k controls the relative intensity of the low-rank constraints on each mode of the restoration result $\mathcal{X}$, which is set by $\alpha_k = \omega_k \sqrt{\frac{I_{\max}}{I_k}}, \quad k \in \{1, 2, 3\}$, here I_k is the size of $\mathcal{X}$ on each mode, $I_{\max} = \max_k(I_k)$; $\omega_1 = \omega_2 = 1$, and $\omega_3 = 100$. After fixing α_k, graph regularization parameter γ_k is tuned accordingly, which makes the HS-MS fusion generalized in various scenes.

The Pavia University dataset[1] is used in our experiments, the top-left $256 \times 256 \times 93$ subimage of dataset is adopted as the reference imagery. Spatial simulation is performed to generate the low-spatial-resolution HSI using 8×8 average PSK $\mathbf{\Psi}$. Spectral simulation is performed to generate the 4-band MSI using an IKONOS-like spectral-response filter as was done in [1]. Three representative tensor based comparison methods are adopted. They are WLRTR [8], CSTF [1] and STEREO [7]. The popular used metrics are defined and can be found in [1, 7].

Table 1. Fusion Performance for the Pavia University Dataset Created Using the 8×8 Average PSK Operator $\mathbf{\Psi}$

	Bicubic	WLRTR[8]	CSTF[1]	STEREO[7]	GLRTA
PSNR	24.56	39.76	43.14	30.96	**44.41**
RMSE	15.1887	3.6484	1.9385	7.7972	**1.7700**
SAM	7.0651	3.5152	2.0315	4.4455	**1.7936**
ERGAS	4.3165	0.9490	0.5423	2.2287	**0.4797**
UIQI	0.5867	0.9772	0.9931	0.9411	**0.9946**
SSIM	0.5699	0.9668	0.9869	0.9316	**0.9906**

Table 1 tabulates quantitative performance of the various algorithms on Pavia University dataset. It can be observed that the proposed GLRTA achieves the best performance. Furthermore, the fusion results are depicted visually in Fig. 2 ; these results include the performance of the HS-MS fusion techniques under consideration as well as simple spatial bicubic interpolation of the HSI to produce a high-resolution HS^{2}I. We further observe that the proposed GLRTA achieves better representation of spatial edge and texture details while more successfully achieving an HS^{2}I with a satisfactory high-spatial resolution and spectrum preservation.

[1] http://www.ehu.eus/ccwintco/index.php?title=Hyperspectral_Remote_Sensing_Scenes

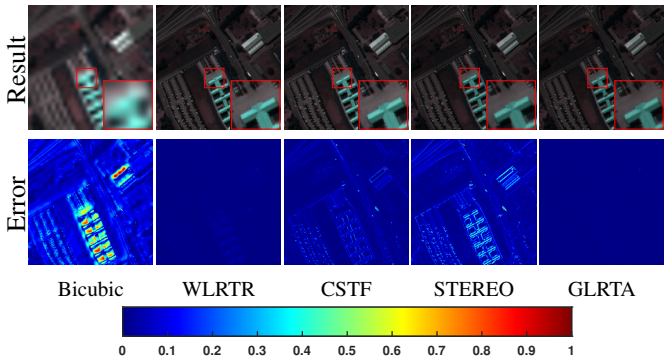

Fig. 2. Pseudocolor (bands 45, 15, and 20) visualization of fusion results; Detailed subimages are enlarged in red squares. "Bicubic" indicates simple spatial bicubic interpolation applied to the HSI; Colorbar gives the scale for the error maps.

Table 2 summarizes the computational complexity of the fusion methods under consideration. All experiments were carried out using MATLAB on an AMD Ryzen 7 5800X 8-Core Processor with 3.80 GHz and with 16 GB of memory. Note that the computational cost of WLRTR is much higher than that of other techniques due to the non-local similarity cubic matching. CSTF has a second slow speed because it needs to learn the dictionaries on each mode. STEREO utilizes an efficient numerical algorithm for solving the Sylvester equation in the fusion model. So, it consumes the least time. However, its fusion performance in (as shown in Table 2) is not that satisfactory. The proposed GLRTA achieves a satisfactory fusion result with significantly less computation than WLRTR and CSTF.

Table 2. Execution Time (In Seconds) for the Selected HS-MS Fusion Methods

Method	WLRTR	CSTF	STEREO	GLRTA
Time	1651.3	84.3	**62.4**	71.6

4. CONCLUSIONS

In this work, a graph-based low-rank tensor approximation (GLRTA) framework has been proposed for HS-MS fusion. Row/column graphs are defined on MSI, and a spectral band graph is defined on HSI to learn the spatial and spectral correlation information. Then, by defining graph smoothness constraints integrated with the low-rank tensor approximation on the fused HS^{2}I, the information learned from the original HSI and MSI are transferred and injected into the final fusion results. Experimental results have demonstrated the superiority of the proposed GLRTA. In the future, we will explore more advanced graph construction strategies to enhance the robustness and generalization of the proposed GLRTA-based HS-MS fusion method.

5. REFERENCES

[1] Shutao Li, Renwei Dian, Leyuan Fang, and José M Bioucas-Dias, "Fusing hyperspectral and multispectral images via coupled sparse tensor factorization," *IEEE Transactions on Image Processing*, vol. 27, no. 8, pp. 4118–4130, August 2018.

[2] Kaidong Wang, Yao Wang, Xi-Le Zhao, Jonathan Cheung-Wai Chan, Zongben Xu, and Deyu Meng, "Hyperspectral and multispectral image fusion via nonlocal low-rank tensor decomposition and spectral unmixing," *IEEE Transactions on Geoscience and Remote Sensing*, vol. 58, no. 11, pp. 7654–7671, November 2020.

[3] Luke Oeding, Elina Robeva, and Bernd Sturmfels, "Decomposing tensors into frames," *Advances in Applied Mathematics*, vol. 73, pp. 125–153, February 2016.

[4] Yang Xu, Zebin Wu, Jocelyn Chanussot, Pierre Comon, and Zhihui Wei, "Nonlocal coupled tensor cp decomposition for hyperspectral and multispectral image fusion," *IEEE Transactions on Geoscience and Remote Sensing*, vol. 58, no. 1, pp. 348–362, January 2019.

[5] Wei He, Yong Chen, Naoto Yokoya, Chao Li, and Qibin Zhao, "Hyperspectral super-resolution via coupled tensor ring factorization," *Pattern Recognition*, p. 108280, 2021.

[6] Ricardo A Borsoi, Clémence Prévost, Konstantin Usevich, David Brie, José CM Bermudez, and Cédric Richard, "Coupled tensor decomposition for hyperspectral and multispectral image fusion with inter-image variability," *IEEE Journal of Selected Topics in Signal Processing*, vol. 15, no. 3, pp. 702–717, April 2021.

[7] Charilaos I Kanatsoulis, Xiao Fu, Nicholas D Sidiropoulos, and Wing-Kin Ma, "Hyperspectral super-resolution: A coupled tensor factorization approach," *IEEE Transactions on Signal Processing*, vol. 66, no. 24, pp. 6503–6517, December 2018.

[8] Yi Chang, Luxin Yan, Xi-Le Zhao, Houzhang Fang, Zhijun Zhang, and Sheng Zhong, "Weighted low-rank tensor recovery for hyperspectral image restoration," *IEEE Transactions on Cybernetics*, vol. 50, no. 11, pp. 4558–4572, November 2020.

[9] Charilaos I Kanatsoulis, Xiao Fu, Nicholas D Sidiropoulos, and Wing-Kin Ma, "Hyperspectral super-resolution via coupled tensor factorization: Identifiability and algorithms," in *2018 IEEE International Conference on Acoustics, Speech and Signal Processing (ICASSP)*. IEEE, 2018, pp. 3191–3195.

[10] Ji Liu, Przemyslaw Musialski, Peter Wonka, and Jieping Ye, "Tensor completion for estimating missing values in visual data," *IEEE Transactions on Pattern Analysis and Machine Intelligence*, vol. 35, no. 1, pp. 208–220, January 2013.

[11] Wei Dai, Ely Kerman, and Olgica Milenkovic, "A geometric approach to low-rank matrix completion," *IEEE Transactions on Information Theory*, vol. 58, no. 1, pp. 237–247, January 2012.

[12] Abhishek Sharma and Maks Ovsjanikov, "Matrix decomposition on graphs: A functional view," *arXiv preprint arXiv:2102.03233*, 2021.

[13] Juliette Valenchon and Mark Coates, "Multiple-graph recurrent graph convolutional neural network architectures for predicting disease outcomes," in *ICASSP 2019-2019 IEEE International Conference on Acoustics, Speech and Signal Processing (ICASSP)*. IEEE, 2019, pp. 3157–3161.

[14] Federico Monti, Michael M Bronstein, and Xavier Bresson, "Deep geometric matrix completion: A new way for recommender systems," in *2018 IEEE International Conference on Acoustics, Speech and Signal Processing (ICASSP)*. IEEE, 2018, pp. 6852–6856.

[15] D. I. Shuman, S. K. Narang, P. Frossard, A. Ortega, and P. Vandergheynst, "The emerging field of signal processing on graphs: Extending high-dimensional data analysis to networks and other irregular domains," *IEEE Signal Processing Magazine*, vol. 30, no. 3, pp. 83–98, May 2013.

[16] Vassilis Kalofolias, Xavier Bresson, Michael Bronstein, and Pierre Vandergheynst, "Matrix completion on graphs," *arXiv preprint arXiv:1408.1717*, 2014.

[17] Yuanyang Bu, Yongqiang Zhao, Jize Xue, Jonathan Cheung-Wai Chan, Seong G Kong, Chen Yi, Jinhuan Wen, and Binglu Wang, "Hyperspectral and multispectral image fusion via graph laplacian-guided coupled tensor decomposition," *IEEE Transactions on Geoscience and Remote Sensing*, vol. 59, no. 1, pp. 648–662, January 2020.

[18] Yang Xu, Zebin Wu, Jocelyn Chanussot, and Zhihui Wei, "Hyperspectral images super-resolution via learning high-order coupled tensor ring representation," *IEEE Transactions on Neural Networks and Learning Systems*, vol. 31, no. 11, pp. 4747–4760, November 2020.

[19] Jian-Feng Cai, Emmanuel Candès, and Zuowei Shen, "A singular value thresholding algorithm for matrix completion," *SIAM Journal on Optimization*, vol. 20, no. 4, pp. 1956–1982, 2010.